*Int. J. Electrochem. Sci.*, 15 **(2020)** 2133 – 2144, doi: 10.20964/2020.03.54

International Journal of
ELECTROCHEMICAL
SCIENCE
www.electrochemsci.org

# Facile Synthesis Of $Fe_2O_3$ Nanospheres Anchored On Oxidized Graphitic Carbon Nitride as a High-Performance Electrode Material for Supercapacitors

*Xiaoyong Zhang, Huiwei Liao*[*], *Xiang Liu, Ronggang Shang, Yu Zhou, Yanna Zhou*

State Key Laboratory of Environment-friendly Energy Materials, School of Materials Science and Engineering, Southwest University of Science and Technology, Mianyang 621010, PR China
[*]E-mail: liaohw6709@163.com

*Received:* 9 November 2019 / *Accepted:* 23 December 2019 / *Published:* 10 February 2020

$Fe_2O_3$, which shows promise as an abundant and low-cost electrode material for supercapacitors has attracted much attention due to its high theoretical specific capacity. In this report, homogeneous $Fe_2O_3$ nanospheres/oxidized g-$C_3N_4$ ($Fe_2O_3$/OCN) are synthesized by anchoring $Fe_2O_3$ nanospheres on the surface of oxidized g-$C_3N_4$ for the first time via a facile hydrothermal method. More importantly, these $Fe_2O_3$ nanospheres are well-dispersed on the oxidized g-$C_3N_4$ layers, which can offer an abundance of active sites and effectively prevent the aggregation of $Fe_2O_3$ nanospheres during electrochemical reactions. Moreover, 10%OCN/$Fe_2O_3$ exhibits excellent electrochemical performance with an excellent specific capacitance of 243 F $g^{-1}$ at a current density of 1A $g^{-1}$, which is better than that of pure $Fe_2O_3$ nanospheres. Moreover, there is no obvious capacitance decrease after 1000 cycles. Therefore, $Fe_2O_3$/OCN is demonstrated to be an excellent electrode material for supercapacitors.

**Keywords:** $Fe_2O_3$ nanospheres; Oxidized graphitic carbon; Electrode material; supercapacitor

## 1. INTRODUCTION

With the excessive development and consumption of energy, exploring a clean, efficient and eco-friendly energy source has becomes increasingly important. Supercapacitors, a high-performance energy storage device, have attracted increasing attention because of their fast charge-discharge rates, high energy and power density and long cycle life[1-3]. Based on the difference of energy storage mechanism, supercapacitor can be divided into an electric double layer capacitor (EDLC) and a pseudo-capacitance. The former stores energy through the adsorption and release of ions between the electrolyte and electrode material, which are composed of C materials such as activated carbon[4], carbon nanotubes[5] and grapheme [6]. Moreover, to increase the utilization efficiency, C materials

have been made into various nanostructures such as nanorods and nanospheres. Pseudo-capacitance stores energy through fast reversible faradaic reactions on the surface of electrode materials, which are composed of conducting polymers and metal oxides such as $RuO_2$[7] and $MnO_2$[8]. By combining the properties of low electrical conductivity and high theoretical specific capacitance from the mental oxides and the high electrical conductivity and large surface area of the C materials, the construction of metal oxides with C materials composites has become an effective method to increase the performance of supercapacitors.

Among these mental oxides, $Fe_2O_3$ is a potential electrode material for supercapacitors because of its high theoretical specific, low toxicity, abundant resources and low cost[9]. To increase the surface of electrode materials and shorten the transport path of ions and electrons, various $Fe_2O_3$ nanostructures have been successfully made by one-pot calcination, hydrothermal, microwave, and reflux to achieve high performance supercapacitors[10-12]. For example, Zhang prepared three-dimensional needle-like $Fe_2O_3$ materials with a specific capacitance of 524.6F $g^{-1}$ at a current density of 1A $g^{-1}$[13]. Although great achievement has been made in supercapacitors, the performance of $Fe_2O_3$ is limited because of its poor electrical conductivity. Therefore, to improve the conductivity, one effective method is to mix $Fe_2O_3$ with C materials.

Graphitic carbon nitride (g-$C_3N_4$), a two-dimensional (2D) graphite-like structure[14-16], has attracted increasing attention because of its high nitrogen content, which can provide more active reaction sites and additional electrons to enhance conductivity and improve wettability with the electrolytes. In addition, mixing a metal oxide with g-$C_3N_4$ as an electrode material is an effective method to improve capacitor performance[17-19]. Usually, there are two methods to address g-$C_3N_4$ for supercapacitors. First, ultrathin g-$C_3N_4$ nanosheets are synthesized using various methods such as a liquid phase stripping method and a high temperature calcination method. More importantly, the metal oxide is anchored on the surface of g-$C_3N_4$ nanosheets. For example, Prabhakar Vattikuti et al. prepared carbon/CuO nanospheres anchored on g-$C_3N_4$ nanosheets as a ternary electrode material for supercapacitors with a specific capacitance of 247.2F $g^{-1}$ at a current density of 1 A $g^{-1}$[20]. Second, g-$C_3N_4$ is oxidized through a the treatment with concentrated acid, and oxidized g-$C_3N_4$ (OCN) possesses abundant oxygen-containing functional groups, such as hydroxyl and carboxyl groups, which can increase the electronic attraction between the $Fe^{3+}$ and oxygen-containing functional groups. However, there are no reports about mixing OCN with metal oxides for supercapacitors.

In this work, $Fe_2O_3$ nanospheres are anchored on the surface of oxidized g-$C_3N_4$ nanocomposites through a facile hydrothermal method for supercapacitor application. Moreover, g-$C_3N_4$ is oxidized through a treatment of concentrated nitric acid. The oxidation treatment of g-$C_3N_4$ through concentrated nitric acid successfully cuts the large layered g-$C_3N_4$ to smaller segments that have a large surface area, which not only increases the edge nitrogen atoms of g-$C_3N_4$ but also introduces much oxygen functional groups that increased the electrostatic interaction between the $Fe^{3+}$ and oxygen-containing groups in g-$C_3N_4$. The composite with 10% $Fe_2O_3$ nanospheres coupled with the oxidized g-$C_3N_4$ exhibits an electrochemical performance with an excellent specific capacitance of 243 F $g^{-1}$, which is better than that of pure $Fe_2O_3$. Moreover, the 10% $Fe_2O_3$/OCN exhibits excellent cycling performance after 1000 cycles.

## 2. EXPERIMENTAL

### *2.1 Chemicals and materials*

All the tests used in the experiments were of analytical grade. Commercial melamine, concentrated nitric acid, methanol and ethanol were purchased from Chengdu Kelong Chemical Co., Ltd. (Chengdu, China). Distilled water was used throughout the whole experiment.

### *2.2. Methods and preparation*

#### *2.2.1. Preparation of g-$C_3N_4$*

g-$C_3N_4$ was synthesized by calcination of melamine in a muffle furnace， which was similar to a reported paper[21]. Briefly speaking, a certain amount of melamine was put into a crucible with a cover, and heated from room temperature to 550 °C with a ramping rate of 3 °C /min; it was held at 550 °C for 2 hours. The yellow product was ground to a powder with an agate mortar.

#### *2.2.2. Preparation of oxidized g-$C_3N_4$*

OCN was synthesized by oxidizing g-$C_3N_4$ with concentrated nitric acid. g-$C_3N_4$ (8 g)was mixed with 500 ml concentrated nitric acid in a beaker. Then, the beaker was transferred to a 40 °C oil bath and heated for 24 h. The oxidized g-$C_3N_4$ was obtained through centrifuge separation and washed with deionized water.

#### *2.2.3. Preparation of $Fe_2O_3$/OCN*

A certain amount of OCN was dispersed in 40 ml of deionized water with ultra-sonication for 10 min .Then 2 g $Fe(NO_3)_3 \cdot 9H_2O$ was added to the OCN solution under magnetic stirring for 30 min at room temperature, and then, 3.5 ml of deionized water was added. Next, 4 g of sodium acetate was added to the above solution for another 1 h stirring. Then, the above solution was transferred into a 50 ml Teflon-lined stainless-steel autoclave for a hydrothermal treatment at 180 °C for 24 h. After naturally cooling to room temperature, the products were obtained through centrifugation and rinsed with deionized water and ethanol several times. Finally, the obtained products were dried at 60 °C in an oven for 24 h. The $Fe_2O_3$/OCN composites with different weight ratios of $Fe_2O_3$ to OCN (2%:1, 10%:1, 15%:1) were prepared by adjusting the content of $Fe_2O_3$ and the corresponding products were named 2%OCN/$Fe_2O_3$, 10%OCN/$Fe_2O_3$ and 15%OCN/$Fe_2O_3$. The obtained $Fe_2O_3$ nanospheres were synthesized by the same step but without adding OCN.

### *2.3. Characterization*

The crystal phase of the as-prepared samples was analyzed by X-ray diffraction (XRD, DMAX1400, Rigaku Corporation, Japan) on an X'- Pert Pro in a 2θ range of 20°-80°. The

morphologies and microstructures of the sample were investigated by using field-emission scanning electron microscopy (FE-SEM, Ultra 55, Carl Zeiss, Germany) and high-resolution transmission electron microscopy (HR-TEM, Libra200, Carl Zeiss Irts, Germany) .The FTIR absorption spectra of the as-prepared samples were measured by a Fourier transform infrared spectrometer (FT-IR5700). X-ray photoemission spectroscopy (XPS) was measured with Axis Ultra DLD Kratos AXIS SUPRA system.

### *2.4. Electrochemical measurement*

The synthesized active materials were mixed with carbon black and polyvinylidene fluoride (PVDF) with a mass ratio of 6:2:2 in N-methyl-2-pyrrolidinone. The mixture was then coated on a clean nickel foam and dried in a heating oven at 60 °C for 12 h. The dried electrode was then pressed using a hydraulic press at a pressure of 10 Mpa to serve as a working electrode.

Electrochemical measurements were measured by using an electrochemical workstation(CHI660B,CHI Shanghai). Cyclic voltammetry (CV), electrochemical impedance spectroscopy (EIS) and constant galvanostatic charge-discharge were performed with a three-electrode cell that consisted of a 2M KOH aqueous solution with a saturated calomel electrode(SCE) and a platinum electrode as the reference electrode and counter electrode. The CV measurement was conducted in a potential window of 0-0.5 V and the GCD measurement was conducted at a potential window of 0-0.46 V. The CV scan rates ranged from 10mV $s^{-1}$ to 100mV $s^{-1}$. Electrochemical impedance spectroscopy (EIS) measurements were performed in a frequency range of 100 kHz-0.01 kHz. The specific capacitance $C_s$ (F $g^{-1}$), energy density (E), and power density (P) were calculated from the discharge curves based on the following equations:

$$C_s = \frac{I\Delta t}{\mathrm{m}\Delta v} \qquad \text{Eq. (A.1)}$$

$$E = \frac{C\Delta \mathrm{v}^2}{7.2} \qquad \text{Eq. (A.2)}$$

$$P = \frac{3600 \times E}{\Delta t} \qquad \text{Eq. (A.3)}$$

Where C is the specific capacitance calculated from the charge-discharge curves, I (A) is the current density, m (g) is the mass of the electrode materials, $\Delta t$ (s) is the discharge time, and $\Delta$v (V) is the applied potential window.

## 3. RESULTS AND DISCUSSION

### *3.1 Characterisation of $Fe_2O_3$/OCN*

The as-prepared samples of the $Fe_2O_3$/OCN composites were characterized by XRD to identity their crystallographic architectures. As shown in Fig. 2a. On the one hand, all characteristic peaks of the $Fe_2O_3$/OCN composites can be indexed to the $Fe_2O_3$ phase with lattice constants a=b=5.0365 and c=13.7489 (JCPDS no. 33-0664), and no other diffraction peaks appeared. On the other hand, the diffraction peaks at 24.1°,33.2°,35.6°,40.9°,49.5°,54.1°,57.6°,62.4°,and 64.0°can be attributed to the

(012) , (014), (110), (113), (024), (116), and (214) planes of $Fe_2O_3$. The diffraction peak at 27.4° can be attributed to the (100) plan of g-$C_3N_4$[22]. There are no other diffraction peaks, which indicate that these samples have high crystallinity and no impurities.

The FTIR spectra of the $Fe_2O_3$/OCN composites are shown in Fig. 2b. The broad band at approximately 3438 $cm^{-1}$ is attributed to the stretching vibration of hydroxyl groups in OCN. The peaks at 465 $cm^{-1}$ and 605 $cm^{-1}$ can be attributed to the lattice absorption of Fe-O, indicating the strong interaction of the $Fe_2O_3$ NPs with the ester O. The sharp intense peak at approximately 808 $cm^{-1}$ is attributed to the breathing vibration of the triazine rings in OCN. In addition, the peaks in the range between 1200- and 1650 $cm^{-1}$ (peaks at 1233, 1389 and 1625 $cm^{-1}$ for OCN), no obvious oxygen functional group-related peaks in the OCN samples.

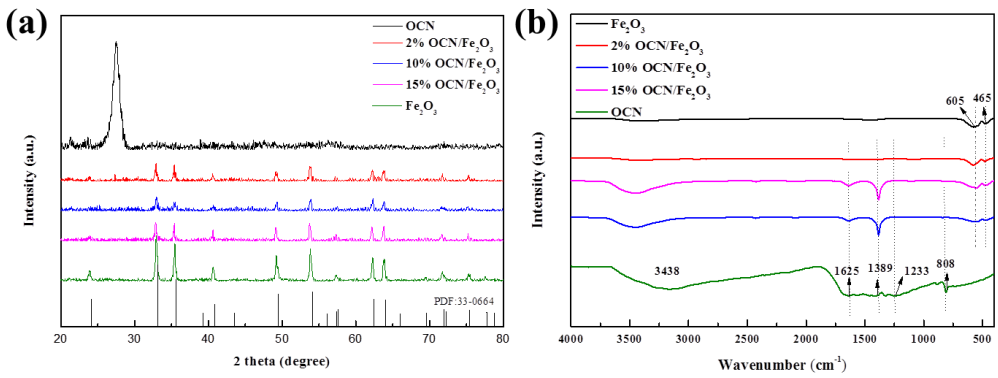


**Figure 2.** XRD analysis (a), FT-IR (b)

As shown in Fig. 1, the oxidation treatment of g-$C_3N_4$ through concentrated nitric acid successfully cuts the larger layered g-$C_3N_4$ to smaller segments, which not only increases the edge nitrogen atoms of g-$C_3N_4$ but also introduces much oxygen functional groups such as hydroxyl (-OH) and amino (-NH) groups. More importantly, these oxygen functional groups can effectively attach to $Fe^{3+}$ because of the electrostatic interaction between the $Fe^{3+}$ and oxygen functional groups after the oxidation treatment of g-$C_3N_4$. Then, $Fe(NO)_3{\cdot}9H_2O$ is added into the OCN solution by magnetic stirring, followed by an addition of sodium acetate . The $Fe(NO)_3{\cdot}9H_2O$ is in-situ hydrolyzed to $Fe(OH)_3$. After that, $Fe_2O_3$ nanospheres are attached to OCN layers ($Fe_2O_3$/OCN) through high-temperature hydrothermal treatment. The reaction mechanism can be described by the following three equations:

$$CH_3COO^- + H_2O \rightarrow CH_3COOH + OH^-$$

$$Fe^{3+} + 3OH^- \rightarrow Fe(OH)_3$$

$$Fe(OH)_3 \rightarrow Fe_2O_3$$

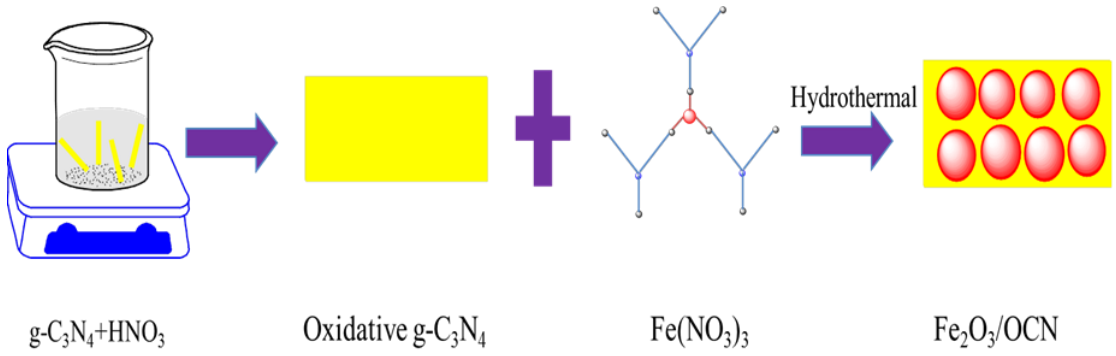


**Figure 1.** Flow chart showing the preparation process for producing homogeneous $Fe_2O_3$ nanospheres coupled with oxidized g-$C_3N_4$.

The morphology and structure of the OCN and 10% $Fe_2O_3$/OCN nanocomposites were measured by SEM analysis. As shown in Fig. 3a, concentrated nitric acid cuts the larger layered g-$C_3N_4$ to smaller segments. From Fig. 3b, Fig. 3c and Fig. 3d, it can be clearly observed that the homogeneous $Fe_2O_3$ nanospheres are well distributed on the surface of OCN. From the HRTEM image in Fig. 4a and Fig. 4b, the black area represents $Fe_2O_3$ nanospheres the well-distributed $Fe_2O_3$ nanospheres on the surface of OCN, which not only prevents the aggregation of the $Fe_2O_3$ nanospheres but also increases the utilization coefficient of the $Fe_2O_3$ nanospheres.

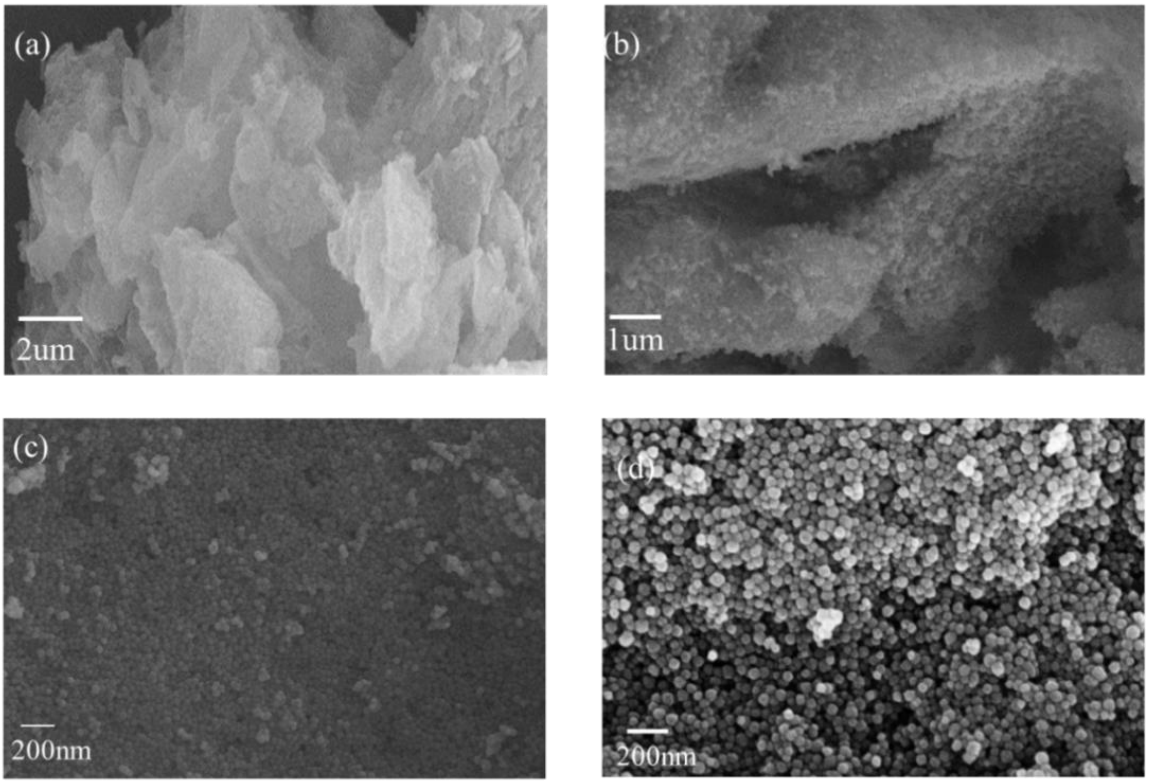


**Figure 3.** FESEM images of the pure oxidized g-$C_3N_4$ (a), and 10% $Fe_2O_3$/OCN (b-d).

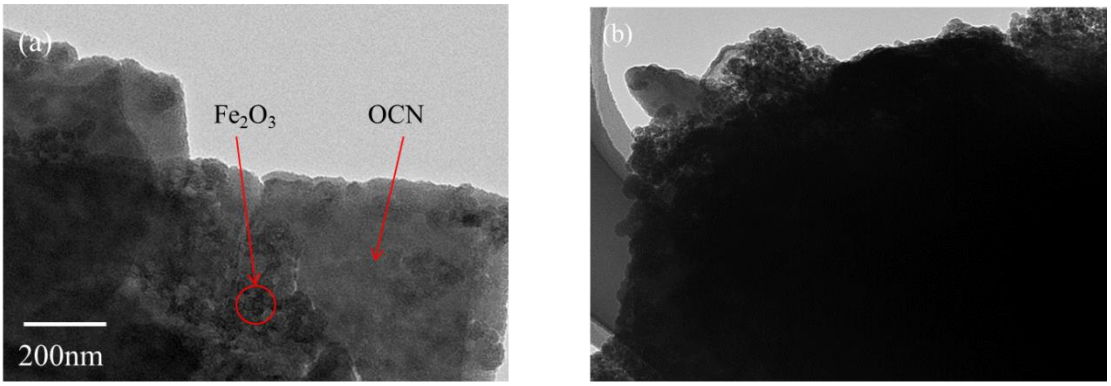


**Figure 4.** TEM images of 10% $Fe_2O_3$/OCN (a-b).

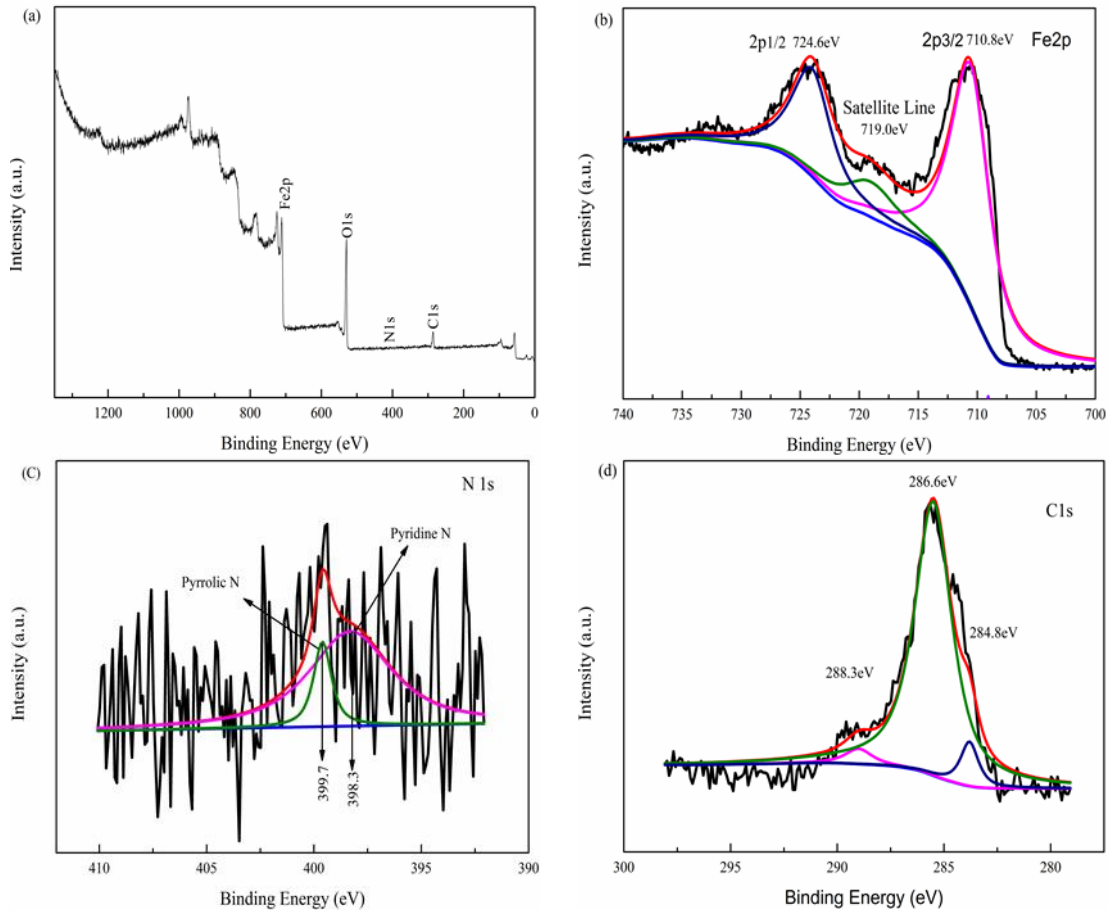


**Figure 5.** XPS spectra survey (a), Fe 2p (b), N 1s (c), C1s (d)

X-ray photoelectron spectroscopy (XPS) analyses were performed. As shown in the Fig. 5a, C, O, N, and Fe elements are observed in the XPS survey spectra of the prepared samples, which corresponds with the elemental mapping images. The characteristic peaks of C, N, O, and Fe centered at approximately 300, 400, 510, and 710 eV. The high-resolution spectrum of the Fe 2p core level in Fig. 5b shows that there are two characteristic peaks centered at 710.8 and 724.6 eV corresponding to the typical values for the characteristic Fe 2p 3/2 and 2p 1/2 peaks[22]. Fig. 5c shows two

characteristic peaks centered at 398.3, and 399.7 eV, which are attributed to pyridinic N and pyrrolic N[23]. In the fig.5d, there are three characteristic peaks centered at 284.8, 286.6 and 288.3 *eV* [24]. The peaks at 284.8 a eV are assigned to the graphitic carbon. And the peak at 286.6 and 288.3 eV are assigned to sp2 C atoms and sp3 C atoms.

### *3.2 Electrochemical performance of $Fe_2O_3$/OCN*

To measure the performance of the $Fe_2O_3$/OCN composites as electrode materials in supercapacitors, we performed an electrochemical test in a 2 M KOH electrolyte with a platinum foil as the counter electrode and a saturated calomel as the reference electrode in a three-electrode system[25]. As shown in Fig. 6a, the cyclic voltammetry tests of pure $Fe_2O_3$, 2% $Fe_2O_3$/OCN, 10% $Fe_2O_3$/OCN, 15% $Fe_2O_3$/OCN were performed at a sweep rate of 50 $mVs^{-1}$. In addition, a couple of redox peaks that can be attributed to the reversible conversion between $Fe^{3+}/Fe^{2+}$ can be found between 0 and 0.5 V. Moreover, compared with pure $Fe_2O_3$ and the other composite materials, 10%OCN/$Fe_2O_3$ have high capacitance at identical sweep rates due to its large surface area; this finding is attributed to two reasons, on the one hand, $Fe_2O_3$ nanospheres possess a large surface area, and on the other hand, the $Fe_2O_3$ nanospheres are uniformly distributed on the surface of the oxidized g-$C_3N_4$.

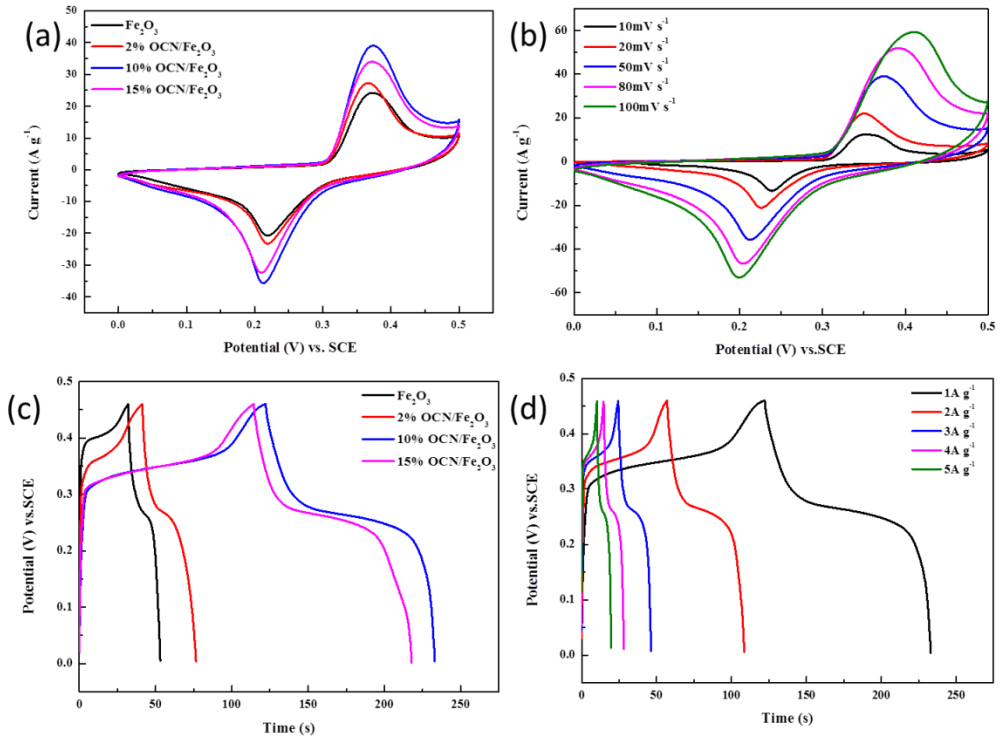


**Figure 6.** CV curves of pure $Fe_2O_3$, 2% $Fe_2O_3$/OCN, 10% $Fe_2O_3$/OCN, and 15% $Fe_2O_3$/OCN (a); CV curves comparison of 10% $Fe_2O_3$/OCN at 50 mv $s^{-1}$ (b); GCD curves at 1A $g^{-1}$ of pure $Fe_2O_3$, 2% $Fe_2O_3$/OCN, 10% $Fe_2O_3$/OCN, and 15%$Fe_2O_3$/OCN (c); and GCD curves Comparison of 10% $Fe_2O_3$/OCN at 1A $g^{-1}$(d)

In addition, different sweep rates between 10 mV $s^{-1}$ and 100 mV $s^{-1}$ of the 10% were applied to 10% $Fe_2O_3$/OCN. It can be seen from Fig. 6b that as the sweep rate increases, the peak current increases, but the shapes of these CV profiles do not alter. More importantly, as the sweep rate increases, the anodic peaks shift to a high potential, while the cathodic peaks shift to a low potential because of the faster charge and discharge rates at high scanning rates. The slight potential shift of the oxidation and reduction peaks can be attributed to the internal charge transfer resistances[26].

The electrochemical performance of the samples was further evaluated by GCD measurements. From the Fig. 6c, the GCD curves are in good agreement with their CV curves. The potential windows of charging and discharging were performed between 0 to 0.46 V and different current densities with 1 A $g^{-1}$,2 A $g^{-1}$, 3 A $g^{-1}$,4 A $g^{-1}$, and 5 A $g^{-1}$ . From the discharging curves, it can be seen that when the current density is 1 A $g^{-1}$, the capacitance of $Fe_2O_3$, 2% $Fe_2O_3$/OCN, 10% $Fe_2O_3$/OCN and 15% $Fe_2O_3$/OCN is 46 F $g^{-1}$, 77 F $g^{-1}$,243 F $g^{-1}$,226 F $g^{-1}$, which demonstrates that 10% $Fe_2O_3$/OCN exhibits much higher specific capacitance than pure $Fe_2O_3$, which can be attributed to the special structure that $Fe_2O_3$ nanospheres are uniformly distributed on the surface of OCN. The reason why 15% $Fe_2O_3$/OCN exhibits a low specific capacitance is the aggregation of $Fe_2O_3$ nanospheres on the surface of OCN. To further investigate the electrochemical performance 10%Fe2O3/OCN, different current densities from 1 A $g^{-1}$ to 5 A $g^{-1}$ were applied. As shown in Fig. 6d, the discharge time decreased with increasing current density, which is attributed to a sluggish reaction because of the fast potential change at a high current density[27]. However, 10% $Fe_2O_3$/OCN exhibits high specific capacitance at a current density of 1 A $g^{-1}$, which is attributed to the fact that ion diffusion can through the high surface area of the composite.

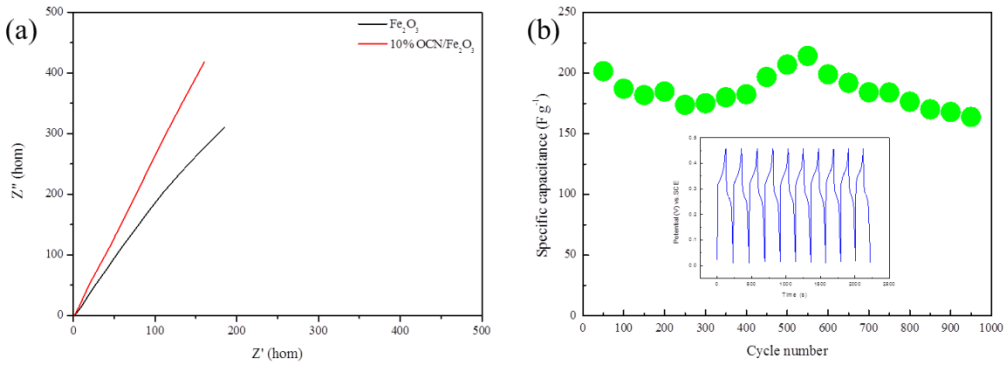


**Figure 7.** Nyquist plot of pure $Fe_2O_3$ and 10% $Fe_2O_3$/OCN (a); and cycling performance of 10% $Fe_2O_3$/OCN (b)

Electrochemical impedance spectroscopy measurements were carried out for the $Fe_2O_3$ nanospheres/OCN electrode. As shown in Fig. 7a, the intercept of the semicircle on the real axis represents the equivalent series resistance (Rs), which is calculated to be 0.652Ω and 0.851Ωfor three electrodes[28]. The electron transfer rate on the electrode surface can be accelerated by combining OCN. As shown in Fig. 7b, the 10% $Fe_2O_3$/OCN shows excellent stability, retaining 81.3% of its original specific capacitance after 1000 cycles. The results indicate that the 10% $Fe_2O_3$/OCN electrode delivers high capacitance good stability for high-performance electrochemical pseudocapacitors. Form

the equations, a maximum energy density of 25.7 7 Wh $kg^{-1}$ can be obtained at a power density of 833.8 W $Kg^{-1}$.

Table 1 describes the published paper about the electrochemical performance of the $Fe_2O_3$-based electrode materials for the supercapacitor. Compared with previous published paper in Table 1, $Fe_2O_3$ nanospheres anchored on oxidized g-$C_3N_4$ exhibit higher specific capacitor than a number of $Fe_2O_3$ nanocomposites.

**Table 1.** Comparison of reported electrochemical performance of the $Fe_2O_3$-based electrode materials

| Electrode | Electrolyte | Specific capacitance | Cycling performance | Refs. |
|---|---|---|---|---|
| $Fe_2O_3$ thin films | 1 M NaOH | 178F $g^{-1}$ (5 mV $s^{-1}$) | - | [29] |
| F-$Fe_2O_3$/AC | 1 M $LiF_6$ | 71 F $g^{-1}$ (2.25 A $g^{-1}$) | 90% for 15000 cycles | [30] |
| a-$Fe_2O_3$ | 1 M LIOH | 256 F $g^{-1}$ (1 mV $s^{-1}$) | 82% for 3000 cycles | [31] |
| a-$Fe_2O_3$ Hollow Nanoshuttles | 1 M KOH | 249 F $g^{-1}$ (0.5 A $g^{-1}$) | 93.6% for 2000 cycles | [32] |
| $Fe_2O_3$ | 1 M KOH | 540 F $g^{-1}$(2.5 A $g^{-1}$) | - | [33] |
| a-FeOOH/$Fe_2O_3$ | 0.1 M $NaSO_4$ | 200 F $g^{-1}$ (5 mA $g^{-1}$) | 99.9% for 500 cycles | [34] |
| $Fe_2O_3$/g-$C_3N_4$ | 2 M KOH | 243 F $g^{-1}$ (1 A $g^{-1}$) | 81.3% for 1000 cycles | This work |

## 4. CONCLUSION

In summary, a composite of homogeneous $Fe_2O_3$ nanospheres coupled with oxidized g-$C_3N_4$ has been synthesized for the first time by a facile hydrothermal method. More importantly, these $Fe_2O_3$ nanospheres are well-dispersed on the oxidized g-$C_3N_4$ layers, which can offer abundant active sites and effectively prevent the aggregation of $Fe_2O_3$ nanospheres during the electrochemical reactions. When used as an electrode material, 10% $Fe_2O_3$/OCN exhibits excellent electrochemical performance with a specific capacitance of 243 F $g^{-1}$. Furthermore, 10% $Fe_2O_3$/OCN presented an excellent cycling performance after 1000 cycles, which can be attributed to its special homogeneous $Fe_2O_3$ nanospheres attached to the surface of oxidized g-$C_3N_4$ that introduced a number of oxygen functional groups, high surface area and low electronic resistance. This study suggests that $Fe_2O_3$/OCN composite can be used as an electrode material for high-performance supercapacitors.

CONFLICTS OF INTEREST

There are no conflicts to declare

ACKNOWLEDGEMENTS
This work was supported by Independent Research Project of State Kay Laboratory of Environmentally Friendly Energy Materials (grant no. 19fksy0112). Also we are grateful for the help of Analytical and Testing Center of Southwest University of Science and Technology.

## References

1. Y.F. Tang, Y.Y. Liu, S.G. Yu, S.C. Mu, S.H. Xiao, Y.F. Zhao, F. Gao, *J. Power Sources*, 256(2014) 160.
2. Y.Q. Qiao, Q.J. Sun, J.Y. Xi, H.Y. Cui, Y.F. Tang, X.H. Wang, *J. Alloys Compd*, 660(2016) 416.
3. Z.Y. Jin, A.H. Lu, Y.Y. Xu, J.T. Zhang, W.C. Li, *Adv. Mater*., 26(2014) 3700.
4. S. Li, W.Y. Pan, Z.Q. Mao, *Int. J. Hydrogen Energy*, 30(2005) 643.
5. Q.F. Xiao, X. Zhou, *Electrochim. Acta*, 48(2003) 575.
6. S. Shahrokhian, R.M. ohammadi, E. Asadian, *Int. J. Hydrogen Energy*, 41(2016) 17496.
7. T.C. Liu, W.G. Pell, B.E. Conway, *Electrochim. Acta*, 42(1997) 3541.
8. P.R. Choi, E. Lee, S.H. Kwon, J.C. Jung, *J. Phys. Chem. Solids*, 87(2015) 72.
9. G. Binitha, M.S. Soumya, A.A. Madhavan, P. Praveen, A. Balakrishnan, K.R.V. Subramanian, M.V. Reddy, S.V. Nair, N. Sivakumar, *J. Mater. Chem*. A, 1(2013) 11698.
10. S. Shivakumara, T.R. Penki, N. Munichandraiah, *Mater. Lett*., 131(2014) 100.
11. X. Zheng, X.Q. Yan, Y.H. Sun, Y.S. Yu, G.J. Zhang, Y.W. Shen, Q.J. liang, Q.L. Liang, Y. Zhang, *J. Colloid Interface Sci*., 466(2016) 291.
12. S.W. Zhang, B.S. Yin, Z.B. Wang, F. Peter, *Chem. Eng. J*., 306(2016) 193.
13. H. Nan, L. Yu, W. Ma, B. Geng, X. Zhang, *Dalton Trans*., 44(2015) 9581.
14. X.X. Wang, J. Chen, X.J. Guan, L.J. Guo, *Int. J. Hydrogen Energy*, 40(2015) 7546.
15. X. Han, D.Y. Xu, L. An, C.Y. Hou, Y.G. Li, Q.H. Zhang, H.Z. Wang, *Int. J. Hydrogen Energy*, 43(2018) 4845.
16. F. Yao, *Int. J. Electrochem. Sci.*, 12(2017) 5951.
17. Y. Zhao, L. Xu, S.Q. Huang, J. Bao, J.X. Qiu, J.B. Lian, l. Xu, Y.P. Huang, Y.G. Xu, H.M. Li, *J. Alloys Compd.*, 702(2017) 178.
18. X. Chang, X. Zhai, S. Sun, D. Gu, L. Dong, Y. Yin, Y. Zhu, *Nanotechnology*, 28(2017) 135705.
19. S.V.P. Vattikuti, P.C. Nagajyothi, PAK. Reddy, M.K. Kumar, J. Shim, B.J.M.R.L. Chan, *Mater. Res. Lett.*, 6(2018) 432.
20. S.V.P. Vattikuti, B.P. Reddy, C. Byon, J. Shim, *J. Solid State Chem.*, 262(2018) 106.
21. X. Chang, X. Zhai, S. Sun, D. Gu, L. Dong, Y. Yin, Y. Zhu, *Nanotechnology*, 28(2017) 135705.
22. S.W. Cao, Y.P. Yuan, J. Fang, M.M. Shahjamali, F.Y.C. Boey, J. Barber, S.C. L. Joachim, C. Xue , *Int. J. Hydrogen Energy*, 38(2013) 1258.
23. B.B. Wei, H.F. Liang, R.R. Wang, D.F. Zhang, Z.B. Qi, Z.C. Wang, *J Energy Chem*, 27(2018) 472.
24. Z.C. Li, L. Wu, L.B. Wang, A.J. Gu, Q.F. Zhou, *Electrochim. Acta*, 231(2017) 617.
25. Y. Yang, B. Zeng, J. Liu, Y. Long, N. Li, Z. Wen, Y. Jiang, *Mater. Res. Innovations*, 20(2016) 92.
26. Z. Chen, J.L. Li, Y. Chen, Y.K. Zhang, G.F. Xu, J. Yang, Y. Feng, *Particuology*, 15(2014) 27.
27. P. Zhao, N. Wang, W.C. Hu, S. Komarneni, *Ceram. Int*., 45(2019) 10420.
28. H.Y. Wang, R.Y. Li, M. Li, Z.J. Li, *J. Alloys Compd*., 742(2018) 759.
29. P.M. Kulal, D.P. Dubal, C.D. Lokhande, V.J. Fulari, *J. Alloys Compd*., 509(2011) 2567.
30. K. Karthikeyan, S. Amaresh, S.N. Lee, V. Aravindan, Y.S. Lee , *Chem Asian J*., 9(2014) 852.
31. G. Binitha, M.S. Soumya, A.A. Madhavan, P. Praveen, A. Balakrishnan, K.R.V. Subramanian, M.V. Reddy, S.V. Nair, A.S. Nair, N. Sivakumar, *J. Mater. Chem*. A, 1(2013) 11698.
32. X. Zheng, X.Q. Yan, Y,H. Sun, Y.S. Yu, G.J. Zhang, Y.W. Shen, Q.J. Liang, Q.L. Liang, Y. Zhang, *J. Colloid Interface Sci*., 466(2016) 291.

33. B.J. Lokhande, R.C. Ambare, R.S. Mane, S.R. Bharadwaj, *Curr Appl Phys*, 13(2013) 985.
34. R. Barik, B.K. Jena, A. Dash, M. Mohapatra, *RSC Adv*., 4(2014) 18827.

© 2020 The Authors. Published by ESG (www.electrochemsci.org). This article is an open access article distributed under the terms and conditions of the Creative Commons Attribution license (http://creativecommons.org/licenses/by/4.0/).